Dissipative particle dynamics simulations for biological tissues: rheology and competition

2011 Phys. Biol. 8 026014

(http://iopscience.iop.org/1478-3975/8/2/026014)

Phys. Biol. **8** (2011) 026014 (13pp) doi:10.1088/1478-3975/8/2/026014

Dissipative particle dynamics simulations for biological tissues: rheology and competition

Markus Basan[1], **Jacques Prost**[1,2], **Jean-François Joanny**[1] **and Jens Elgeti**[1]

[1] Laboratoire Physico-Chimie Curie Institut Curie Centre de Recherche, CNRS-UMR 168, UPMC Paris VI, 26 rue d'Ulm, F-75248 Paris Cedex 05, France
[2] ESPCI ParisTech, 10 rue Vauquelin, F-75231 Paris Cedex 05, France

E-mail: basan.markus@gmail.com and jens@elgeti.de

Received 29 September 2010
Accepted for publication 4 March 2011
Published 1 April 2011
Online at stacks.iop.org/PhysBio/8/026014

Abstract
In this work, we model biological tissues using a simple, mechanistic simulation based on dissipative particle dynamics. We investigate the continuum behavior of the simulated tissue and determine its dependence on the properties of the individual cell. Cells in our simulation adhere to each other, expand in volume, divide after reaching a specific size checkpoint and undergo apoptosis at a constant rate, leading to a steady-state homeostatic pressure in the tissue. We measure the dependence of the homeostatic state on the microscopic parameters of our model and show that homeostatic pressure, rather than the unconfined rate of cell division, determines the outcome of tissue competitions. Simulated cell aggregates are cohesive and round up due to the effect of tissue surface tension, which we measure for different tissues. Furthermore, mixtures of different cells unmix according to their adhesive properties. Using a variety of shear and creep simulations, we study tissue rheology by measuring yield stresses, shear viscosities, complex viscosities as well as the loss tangents as a function of model parameters. We find that cell division and apoptosis lead to a vanishing yield stress and fluid-like tissues. The effects of different adhesion strengths and levels of noise on the rheology of the tissue are also measured. In addition, we find that the level of cell division and apoptosis drives the diffusion of cells in the tissue. Finally, we present a method for measuring the compressibility of the tissue and its response to external stress via cell division and apoptosis.

S Online supplementary data available from stacks.iop.org/PhysBio/8/026014/mmedia

1. Introduction

The development of tissues is an essential property that distinguishes complex multicellular species from cultures of unicellular organisms. In vertebrate tissue, single cells sacrifice the optimization of their individual growth rate for the well-being of the entire organism, by performing specialized beneficial functions.

Understanding the collective behavior of eukaryotic cells constituting a tissue is therefore of central importance for a variety of biological fields from embryogenesis to tumor progression. In studies of tissues, emphasis has often been put on signalling pathways. However, it has recently become clear that mechanical effects play an important role in the growth and development of biological tissues. At the single cell level, mechanical stresses couple to the orientation of the mitotic spindle during cell division [1]. Pressure has also been shown to strongly influence the expression of some genes for example during drosophila development or in tumors [2]. Finally, there is now a large body of evidence suggesting that cell differentiation depends on the mechanical properties of the substrate, in particular the value of its elastic modulus [3].

A macroscopic description of the mechanical or rheological properties of tissues requires a constitutive equation which relates the local stress in the tissue to the strain or the strain rate. An intuitive approach is to consider

a tissue as an elastic solid, for which the stress only depends on the local strain at a given time, in general in a nonlinear way. The nonlinear elastic description of tissues has been very successful, for example, in explaining growth instabilities of plant tissues. In a completely opposite limit, following the seminal works of Steinberg and coworkers [4–6], it has been argued that during early development, many tissues should be considered as liquids with a finite viscosity and an isotropic surface tension. Between these two regimes, any intermediate complex fluid behavior is of course possible and in certain situations, tissues have been described as visco-elastic or plastic materials. The precise mechanical description of tissues is still a matter of debate and it is therefore interesting to further investigate the rheological response of tissues to external forces [7, 8].

In an earlier work [9], we followed this line of thought and argued that tissues can effectively be treated as viscous fluids on the timescales of growth. We used these ideas to suggest that mechanical competition due to the homeostatic growth pressure is an important part of tumor growth. The homeostatic state is defined as the steady state reached by a tissue when it is allowed to grow in a finite volume with no restriction on nutrients and growth factors. Using a continuum hydrodynamic description of tissues, we studied several biological questions including the origin of metastatic inefficiency [9] and fingering instabilities frequently observed at the stromal–epithelial interface [10]. More recently, we investigated the effect of cell division and apoptosis on tissue rheology [11]. While several studies show that many tissues such as embryonic epithelial tissues behave as viscous fluids [4–6], we argue that tissues, which are completely elastic at short times, undergo fluidization due to coupling between stress and the cell division-apoptosis rate, which relaxes residual stress and leads to a visco-elastic behavior with a relaxation time of the order of the inverse rate of cell turnover.

In this paper, we use a particle-based tissue simulation technique based on a few intuitive assumptions about single-cell behavior to study the macroscopic properties of tissues such as their rheology. Our simulation leads to a well-defined homeostatic state and naturally gives rise to pressure-based tissue competition. We also discuss the role of cell division and apoptosis on tissue fluidization as introduced in our earlier work [11] and present additional data on this effect.

Particle-based simulations have been extensively used to study complex fluids such as colloidal suspensions or polymer melts. They have also already been implemented to study the dynamics of biological tissues taking into account cell division, apoptosis, and active forces. In most of the particle-based tissue simulations, Langevin dynamics models were employed, for example, we refer to the numerous works by the group of Drasdo [12–21].

Early particle-based tissue simulations were conceived for understanding simple *in vitro* experiments with two-dimensional cell populations spreading on a substrate. The growth curves in these experiments were extensively studied by Bru *et al* [22, 23]. In these simulations, the cells take the form of dumbbells during cell division and the orientation of the division axis is in the direction of the maximum force exerted on the cell. The adhesive interactions between cells are described by a pair potential based on the Johnson–Kendall–Roberts (JKR) approximation, which gives the interaction force between two adhesive spheres. The Langevin equations of motion are obtained by balancing the friction forces arising from the interaction with the substrate with external compression forces, adhesion forces and random forces due to cellular movement.

The growth of three-dimensional cell aggregates has also been investigated extensively using particle-based models [15, 16, 24]. Experimental results on the growth of tumor spheroids limited in size by nutrients such as oxygen and glucose have largely been reproduced in these simulations [25, 26]. In a somewhat different approach, more biological details of individual cells have been incorporated by modeling a cell as a multi-particle structure [27, 28]. For example, Sandersius and Newman investigate tissue rheology with a variety of computer experiments.

In the following, we use a similar idea and describe each cell as two repelling particles. We first introduce our simulation model in section 2. Then, we discuss growth and homeostatic state in section 3. Tissue surface tensions and cell sorting are discussed in section 4. The last two sections are devoted to the diffusion of cells inside the tissue (section 5) and the rheological properties of the simulated tissues (section 6). The paper ends with a summary and a discussion of our main results.

2. Tissue simulations

In this work, we use a minimalist approach to model cells and tissue growth. By this, we mean that we use a simple model that fulfills a certain set of requirements for the tissue. In particular, our simulated cells should

- readily adhere to each other,
- maintain volume exclusion,
- exert an active growth pressure on their surrounding,
- expand in size until reaching a size checkpoint,
- divide when reaching this size checkpoint,
- undergo apoptosis,
- exert random forces on neighboring cells,
- regulate to their homeostatic state via cell division and apoptosis in a confined volume,
- give rise to tissue surface tension,
- comply with force balance and momentum conservation.

The model that we present here—though simple and purely mechanical—fulfills all of the above requirements.

2.1. Individual cells

Based on experimental evidence [29], we assume that a given cell type has a particular size checkpoint, which it must overcome in order to enter mitosis. To describe cell growth, we use a model in which each cell consists of two particles i and j interacting via a repulsive growth force $\vec{F}_{ij}^{G}$. The distance between the two particles, constituting the same cell, represents the cell's size. When the distance between the cell

particles exceeds a size threshold R_c, the cell divides. To create the new cell, particles must be inserted. After the division, each of the original particles belongs to a different cell. The new particles are then placed randomly within a short distance r_c from the particles of the original cell. In some simulations, we impose vanishing cell division by setting $\vec{F}_{ij}^{G} = 0$ and R_c large. While cell division is implemented in this deterministic manner, apoptosis (and other forms of cell death) is included by removing cells randomly at a constant rate k_a. For the interaction between cells (adhesion and volume exclusion), forces are defined between the cell particles i and j that do not belong to the same cell. These interact via a short range repulsive force $\vec{F}_{ij}^{CC}$ and a constant attractive force $\vec{F}_{ij}^{a}$ if they are within a certain range of each other.

The total conservative force $\vec{F}_i$ acting on particle i is thus

$$F_i = F_{ic}^{G} + \sum_j \left(\vec{F}_{ij}^{CC} + \vec{F}_{ij}^{a}\right) \tag{1}$$

where the sum runs over all particles j except for the particle belonging to the same cell c.

2.2. Energy dissipation

Energy is dissipated by using a dissipative particle dynamics (DPD) type thermostat [30] on the particles. DPD is a widely used simulation technique to study hydrodynamics of complex fluids. Details about implementing DPD are readily available in the literature [30]. Here, we just note some features that are of particular importance for our simulations: the DPD algorithm introduces viscous dissipation between cells, while preserving momentum balance. The dissipative force reads

$$F_i^{D} = -\gamma\omega(r_{i,j})((v_j - v_i)r_{ij})\hat{r_{ij}} \tag{2}$$

where $\vec{r}_{ij} = \vec{r}_j - \vec{r}_i$ is the vector between the particles i and j located at $\vec{r}_i$ and $\vec{r}_j$, respectively. The modulus and direction of $\vec{r}_{ij}$ are denoted by r_{ij} and $\hat{r}_{ij}$, respectively. A similar notation holds for the velocity $\vec{v}_i$. ω is a weight function (for more details, see [30]). Since cells consist of two particles in our model, the dissipation constants between particles of different cells γ_t and between the particles constituting the same cell γ_c can be chosen independently. We also implement a background dissipation γ_b to model the effect of an extracellular matrix. Because we are mainly interested in studying tissues without bulk extracellular matrix such as epithelia, we typically set this dissipation coefficient to very low values (about three orders of magnitude smaller than γ_c[3]) in our simulations.

At the cost of higher numerical complexity, the major advantage of DPD versus Langevin simulations is that DPD does not assume the background dissipation to be the dominant mode of dissipation. Indeed, in epithelial tissues, where the extracellular matrix is typically absent, dissipative forces are transferred to neighboring cells and not to the background. In our simulation, a random force is added in addition, which mimics motility forces from the cytoskeleton. The noise amplitude $k_B T_n$ is associated with an effective temperature and for equilibrium systems fulfills the Stokes–Einstein relation. Regarding weight functions and integrators, we follow method 3.1 of [30].

[3] Cell division and apoptosis break momentum balance. In simulations where momentum cannot be dissipated to the boundaries, a small background dissipation is thus needed.

2.3. Interaction forces

To reduce the number of parameters, we use simple central forces. The force F_{ij}^{G} felt by particle i due to particle j belonging to the same cell and driving the expansion of that cell is proportional to the growth coefficient B. F_{ij}^{G} is given by

$$F_{ij}^{G} = \frac{B}{(r_{ji} + r_0)^2}\hat{r}_{ji}. \tag{3}$$

For adhesion and volume exclusion between cells, equivalent forces are defined between cell particles. Volume exclusion of cells is modeled by a repulsive force on particles constituting different cells of the form

$$F_{ij}^{CC} = \begin{cases} f_0\left(R_{pp}^5/r_{ji}^{-5} - 1\right)\hat{r}_{ji} & \text{if} \quad r_{ji} \leqslant R_{pp} \\ 0 & \text{if} \quad r_{ji} > R_{pp}. \end{cases} \tag{4}$$

Finally, adhesion is implemented via a constant force $\vec{F}_{ij}^{a} = -f_1\hat{r}_{ji}$ between particles of different cells within a range $r_{ij} \leqslant R_{pp}$, with f_0 and f_1 the repulsive and attractive cell–cell potential coefficients, respectively.

We find that tissue behavior on large scales does not depend on the details of the interaction forces, consistent with results by Drasdo *et al* [19]. With these three forces and our basic division and apoptosis rules, we arrive at a minimalistic tissue model. Although interactions in real tissues are much more complex, we argue that some fundamental and universal properties of tissues are captured with this approach.

2.4. Standard tissue and units

To facilitate the comparison of different simulations, we define a standard tissue (see table 1) which we use as a starting point to explore parameter space. Well-defined, measurable properties of the standard tissue are chosen to rescale data and parameters for comparison with experiments. All values and numerical figures presented in this work without further comments are given in terms of these units. Values can be converted to SI units using table 2. An asterisk * denotes quantities normalized by the corresponding value in the standard tissue (e.g. $B^* = B/B_{ref}$).

As a unit of time t^{ref}, we use the inverse growth rate of the unconfined standard tissue. The unit length l^{ref} is defined by the effective cell diameter $l^{ref} := 2(3/(4\pi\rho)^{1/3}$ in the standard tissue at its homeostatic state. The cell number density ρ for this definition is measured in periodic boundary conditions with box lengths 5.59. Finally, we use the homeostatic pressure of the standard tissue grown in a double plate compartment as the unit stress p^{ref}.

3. Growth, competition and homeostatic state

3.1. Tissue growth

When unconfined by compartment walls or lack of nutrients, the tissue grows exponentially forming a spheroid (see

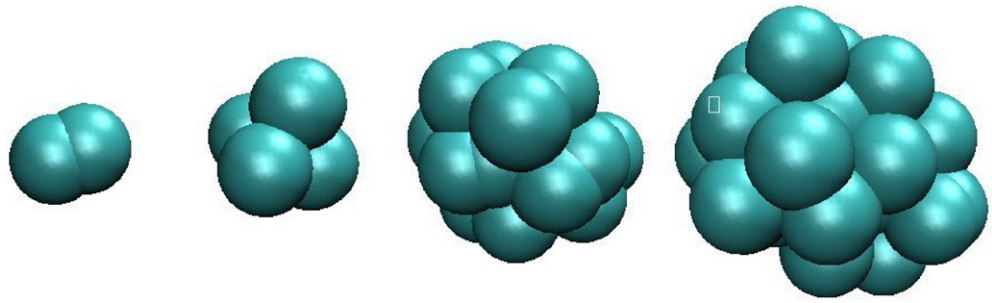

Figure 1. Each cell consists of two particles that repel each other with an intracellular expansion pressure given by equation (3). The intracellular damping coefficient γ_c fixes the timescale of cell division. When the distance between the two particles exceeds a certain threshold R_c (a 'size checkpoint'), the cell divides and two new particles are inserted a small distance r_c away from the old ones in random directions (visualization using VMD [38]). With permission from [11].

Table 1. DPD standard tissue parameters—parameters used for the standard tissue. The plots in the main text are normalized with respect to this tissue.

Parameter	Value	Unit	Description
B	2.37	$p^{\mathrm{ref}}\ (l^{\mathrm{ref}})^4$	Growth coefficient
r_0	1.12	l^{ref}	Cellular expansion pressure constant II
γ_c	4.42×10^{-1}	$p^{\mathrm{ref}}\ l^{\mathrm{ref}} t^{\mathrm{ref}}$	Intracellular dissipation constant between particles of the same cell
γ_t	2.21×10^{-1}	$p^{\mathrm{ref}}\ l^{\mathrm{ref}}\ t^{\mathrm{ref}}$	Intercellular dissipation constant between particles of different cells
γ_b	4.42×10^{-4}	$p^{\mathrm{ref}}\ l^{\mathrm{ref}}\ t^{\mathrm{ref}}$	Background dissipation coefficient in Forceshear simulations $\gamma_b = \gamma_t/10$
R_t	1.12	l^{ref}	Range of dissipative dissipation forces
k_a	7.67×10^{-2}	$(t^{\mathrm{ref}})^{-1}$	Rate of cell death
R_c	8.95×10^{-1}	l^{ref}	Distance threshold for cell division
r_c	1.12×10^{-5}	l^{ref}	Distance at which new particles are placed when the cell divides
$k_B T_n$	4.24×10^{-3}	$p^{\mathrm{ref}}\ (l^{\mathrm{ref}})^3$	Noise intensity in the tissue
f_0	9.08×10^{-2}	$p^{\mathrm{ref}}\ (l^{\mathrm{ref}})^2$	Repulsive cell–cell potential coefficient
f_1	1.90×10^{-1}	$p^{\mathrm{ref}}\ (l^{\mathrm{ref}})^2$	Attractive cell–cell potential coefficient
R_{pp}	1.12	l^{ref}	Range of pair potentials
m	5.76×10^{-4}	$p^{\mathrm{ref}}\ (t^{\mathrm{ref}})^2\ l^{\mathrm{ref}}$	Cell particle mass
dt	1.3×10^{-4}	t^{ref}	Integration timestep

Table 2. Rescaling units—suggestions for the standard tissue scales in real physical units. This table can be employed to convert quantities presented to real units.

Parameter	Value	Description
t^{ref}	1 day	Inverse unconfined growth rate of standard tissue
l^{ref}	10 μm	Particle diameter in homeostatic standard tissue
p^{ref}	1000 Pa	Homeostatic pressure of standard tissue

figure 1). The cell division timescale depends on simulation parameters, but is dominated by B/γ_c in realistic parameter regimes. As the spheroid becomes large, cell growth is hindered by neighboring cells. In the bulk of the tissue, cells must deform the surrounding tissue to increase their volume in order to divide. Terming the total resistance felt by the cell particles due to their surrounding γ_η, to a first approximation, the division timescale in the bulk is then proportional to $(\gamma_c + \gamma_\eta)/B$. Thus, the division rate in the bulk is smaller than at the surface.

At high levels of adhesion, this effect can become so severe that cell division is unable to balance cell death. In this case, the bulk tissue is not viable and undergoes net apoptosis. Cells that are close to the free surface are less constrained by their neighbors and divide close to their unconstrained rate, replenishing the tissue. This leads to the existence of a stable steady state, where average surface cell division balances bulk apoptosis. The division and apoptosis rates per unit volume given by $\rho \cdot k_d$ and $\rho \cdot k_a$, respectively, are shown as a function of the radial location r in steady-state tissue aggregates in figure 2. We see that cell division events are localized at the surface of the tissue and that almost no cell division occurs in the bulk. It should be emphasized that this phenomenon is limited to parameter regimes with strong adhesion, small growth force and large apoptosis. Whether or not such steady states are physiologically relevant is an interesting question that should be addressed in the future. We do not consider this regime in the remainder of this paper.

3.2. Homeostatic pressure

The homeostatic pressure of the tissue is defined as the mechanical pressure that a tissue grown in a finite compartment develops on the compartment walls, when not limited by lack of nutrients or growth factors, as discussed in an earlier work [9]. A tissue, not limited by nutrients, grows to fill the available volume completely. The homeostatic state of the tissue is defined by a balance of cell division and apoptosis; this is thus a stable fixed point of tissue growth dynamics [9].

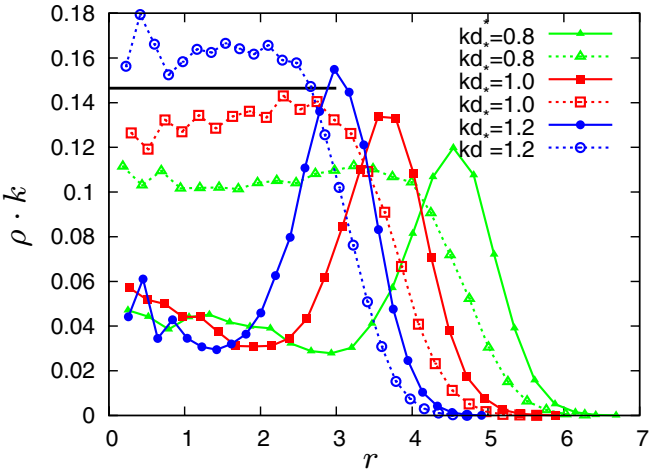

Figure 2. Cell division (solid lines and symbols) and apoptosis (dashed line, open symbols) rates per volume as a function of radial position in an adhesion-limited, steady-state tissue spheroid. The solid black line segment indicates the bulk per-volume death rate of the standard tissue. To obtain such a steady-state cluster size, we employ a reduced intracellular repulsion by setting $B^* = 0.4$. All other parameters are those of the standard tissue given in table 1. Cell division takes place close to the tissue surface, while almost no cells are able to divide in the bulk of the tissue. Note that the apoptosis rate per cell is constant by construction. The drop in the apoptosis rate per volume at the surface of the spheroid seen in the plot is due to decreased cell density.

When confined in a finite volume, the model tissue introduced in this work approaches a well-defined homeostatic state, characterized by a well-defined pressure, which can be measured in the simulation. For quantitative measurements of this pressure, the tissue is grown in a box with two parallel hard walls and periodic boundary conditions in the other directions. This parallel plate simulation allows for a pressure measurement without interference from surface tension effects, by determining the momentum exchange with the bounce-back walls.

Figure 3 shows the dependence of the homeostatic pressure and density on important model parameters. From figure 3(*C*), it is apparent that the homeostatic pressure of the tissue is dominated by the cellular growth coefficient given by B (equation (3)). Increasing the apoptosis rate k_a (figure 3(*A*)) reduces the steady-state density in the tissue and therefore decreases the homeostatic pressure. When the apoptosis rate is too large, cell growth is unable to replenish the tissue, the homeostatic state no longer exists and the tissue dies as shown above (see section 3.1). As demonstrated in the previous section, the cell–cell adhesion force F_a (figure 3(*B*)) directly hinders growth, and therefore reduces the homeostatic pressure. The contribution of the noise intensity to the homeostatic pressure is small compared to that of the cellular growth coefficient for $B^* = 1.0$ and $B^* = 1.5$. However, for small growth coefficients, such as $B^* = 0.5$, for instance, the random forces in the tissue can be the dominant contribution to homeostatic pressure. Changes in the intercellular damping coefficient γ_t in the range $0.02 < \gamma_t^* < 2$, plotted in figure 3(*E*), do not appear to affect the homeostatic pressure of the tissue. This is because the intracellular dissipation γ_c is the dominant mode of dissipation that limits the speed of cell division. Indeed, figure 3(*F*) shows that the intracellular dissipation γ_c does have a small effect on the homeostatic pressure. Increasing the intra-cellular dissipation γ_c slows down the rate of cell division, making the tissue less efficient in filling the space created by the constant rate of apoptosis. In turn, this lowers the cell density and decreases the homeostatic pressure.

3.3. Tissue competition

In [9], we predicted that the homeostatic pressure is an essential concept for understanding tissue competition in a finite compartment. Confirming our earlier hypotheses, we show that for two tissues grown in competition for the same volume, the tissue with the higher homeostatic pressure takes over the compartment. To initialize a tissue competition simulation, in a compartment filled with a tissue at its homeostatic state, a single cell is mutated to a second tissue type of higher homeostatic pressure. In general, the new tissue takes over the compartment completely. Note that it is the homeostatic pressure and not for example the division rate that determines the outcome of this process. Indeed, a tissue with lower division rate, but a higher homeostatic pressure, wins the competition (see figure 4). This is a conceptually important point: contrary to what is commonly accepted, the cell division and apoptosis rates in the absence of stress are not sufficient to predict the result of tissue competition experiments. Our simulations clearly show that the determining parameter is indeed the homeostatic pressure. Note that in this section we choose the physical properties of the two tissues such that the interfacial tension (as discussed below) is small enough to have only a negligible effect.

4. Surface tension and cell sorting

As shown in many experimental works, the presence of surface and interfacial tensions is a generic property of biological tissues. Steinberg and others have shown that tissues behave like viscous liquids with interfacial tensions [4–6]. In particular, droplets of tissues do not only round off to approach a spherical shape, but mixtures of tissue types with different adhesive properties unmix and the less adhesive tissue spreads over the surface of the more adhesive one. Cell–cell adhesion is closely related to the surface tensions measured in experiments such as the double plate compression of a tissue droplet. A direct correspondence between adhesive properties and tissue surface tension has been suggested by Steinberg with the 'differential adhesion hypothesis' [31].

In our simulations, we observe that unconfined tissue aggregates round up to assume spherical shapes. To measure the surface tension, a freely growing tissue is placed in a harmonic potential of stiffness k along the z-direction $V(z) = kz^2/2$. This forces the tissue to grow in a pancake-like shape. The surface tension σ_S can then be found as follows: the free energy in the central area A of the pancake is given by

$$F = A \int \rho(z) V(z)\, \mathrm{d}z + 2\sigma_S A. \qquad (5)$$

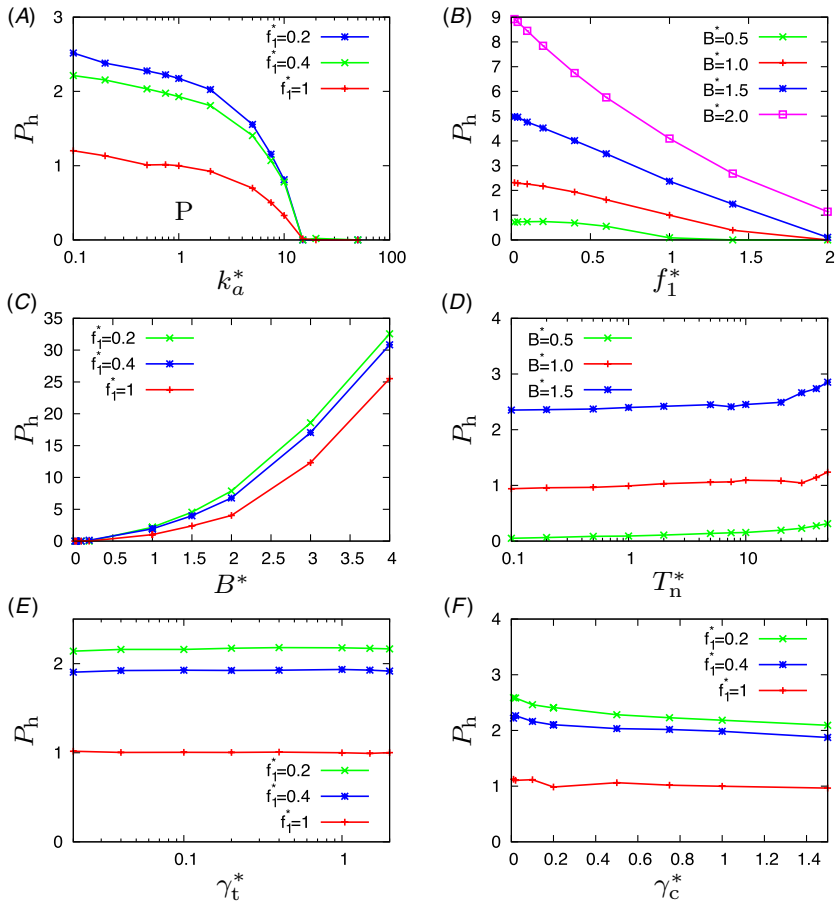

Figure 3. Dependence of the homeostatic pressure P_h on the following parameters is shown: (*A*) apoptosis rate k_a^*, (*B*) adhesion coefficient f_1^*, (*C*) cellular growth coefficient B^*, (*D*) noise intensity T_n^*, (*E*) intercellular DPD damping coefficient γ_t^*, (*F*) intracellular DPD damping coefficient γ_c^*. All microscopic parameters are given relative to their value in the standard tissue (table 1) as indicated by the asterisk. Each pressure point was measured by growing a tissue in a finite compartment of dimensions $L_x = L_y = L_z = 5.59$ and fitting the steady-state pressure after the initial growth phase with a constant.

Assuming that ρ is constant over the thickness of the pancake d, and minimizing the free energy at constant volume, we obtain

$$\sigma_S = \frac{\rho k d^3}{24}. \tag{6}$$

It should be emphasized that this ignores any dynamic contributions to the pancake thickness and assumes that the configuration of the tissue has had time to equilibrate. In the supplementary information, we verify that these effects are small for the studied cases (supplementary figure 5 available at stacks.iop.org/PhysBio/8/026014/mmedia). We work at a lower cell division rate (increased γ_c) and verify the invariance of the measured surface tension under variations of γ_c. In the simulation, we then measure the quantity $\zeta = \sum_i z_i^2 / (\pi r_0^2)$ within a central region of radius $r_0 = 3R_{\mathrm{pp}}$ (z_i denotes the z-component of $\vec{r}_i$). To minimize dynamic contributions, the measurement is performed in the time frame, where the number of cell particles ranges from 100 to 4000. In the continuum limit, ζ is found by integrating over the volume

$$\zeta = \int_0^{r_0} r\,\mathrm{d}r \int_0^{2\pi} \mathrm{d}\phi \int_{-\infty}^{\infty} \mathrm{d}z\, \rho(z)\, z^2 / (\pi r_0^2) = \rho d^3/12 \tag{7}$$

and thus

$$\sigma_S = k\zeta/2. \tag{8}$$

Figure 5 shows ζ as a function of k^{-1}. Consistent with the above calculations, ζ scales essentially linearly with k^{-1}. The resulting surface tension increases linearly with adhesion parameter f_1.

To further test the applicability of our simulation approach, we perform tissue sorting simulations based on differences in surface tensions. We show that the cell sorting experiments described above can be reproduced. To initialize a cell sorting simulation, we grow an unconfined spheroid of tissue and change a given fraction of the cells into a second tissue type with different adhesive properties in a random fashion. We also set cell division and apoptosis to zero. At low adhesion strength, the random forces present in the tissue induce the merging of the cells into larger and larger clusters even in the absence of cell division. The progression of a cell sorting simulation with a reduced level of adhesion is illustrated in figure 6 with two snapshots at different simulation times. As in the mentioned experiments, the stronger adhering tissue aggregates in the center of the spheroid. Clearly, the

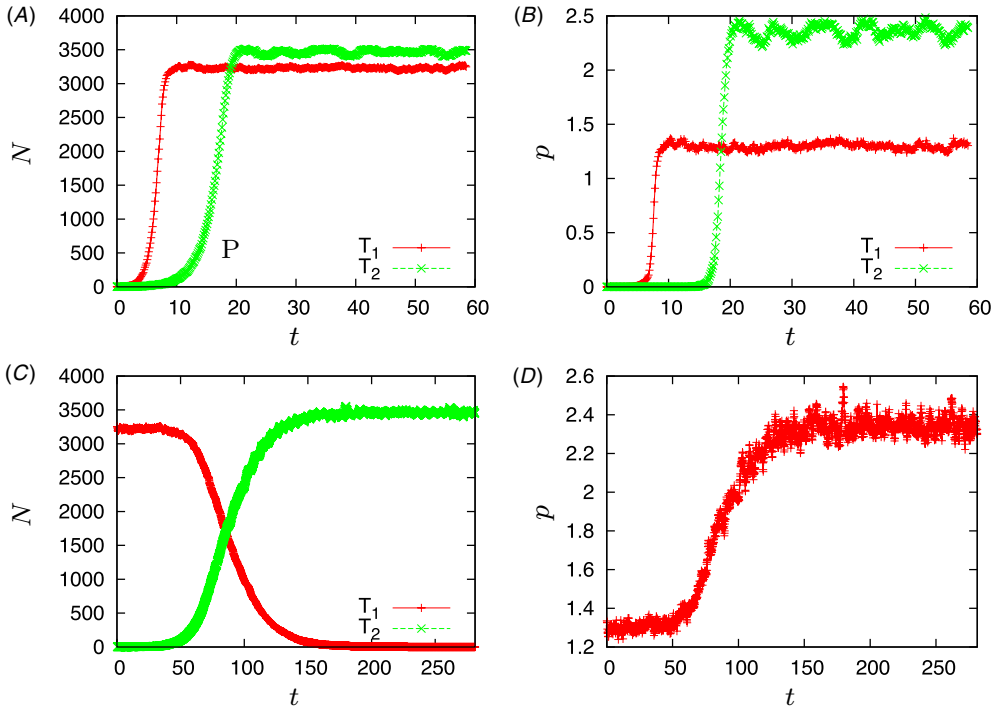

Figure 4. (A) Number of cells N as a function of time t for two different tissue types *grown independently* in a cubic compartment of size $L = 11.2$. The compartment consists of two parallel plates and periodic boundary conditions in the other directions. While the standard tissue T_1 has the standard growth coefficient $B^* = 1.0$ and an intracellular damping coefficient $\gamma_c^* = 1.0$, the second tissue type T_2 has a higher growth coefficient $B^* = 1.5$, but also a higher intracellular damping coefficient $\gamma_c^* = 4.0$. Noise is increased to $k_B T_n^* = 10.0$. As it is visible from (A), T_2 has a lower unconfined growth rate than T_1. (B) Plot of the pressure measured by the compartment wall in the same simulations as in (A) as a function of time. The second tissue T_2 has a higher homeostatic pressure than T_1. (C) Plot of the number of cells of the two species *in competition*. The second tissue T_2 takes over the entire compartment. (D) Plot of the pressure measured by the compartment wall in the competition simulation shown in (C).

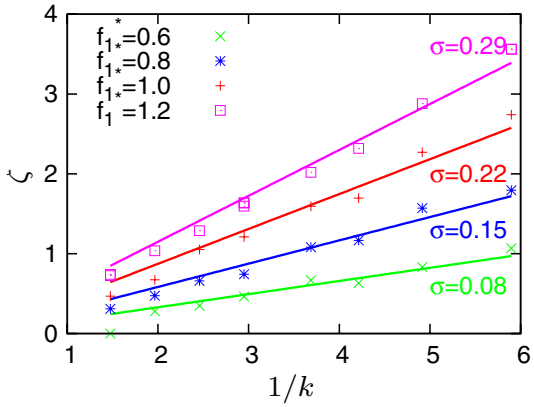

Figure 5. The quantity ζ (as defined in the main text) as a function of the inverse stiffness of the confining potential $1/k$ for various adhesion coefficients f_1. Cell division is slowed down but expansion is strong by setting $\gamma_C^* = 5$ and $B^* = 2$. All other parameters are the same as in the standard tissue. As shown by the linear fits (solid lines), the linear relationship predicted by equation (8) is well reproduced.

presence of adhesive interactions between the cells in our simulation gives rise to tissue surface and interfacial tensions.

5. Diffusion of cells within the tissue

The diffusion constant of cells within tissues has been investigated in several experimental studies [32–34], showing that cells perform a persistent random walk and that the diffusion constant is smaller in more cohesive aggregates than in less cohesive ones. In our simulations, the diffusion constant of cells inside the tissue can easily be determined by measuring their mean squared displacement over time. Increasing adhesion between cells slows down diffusion as expected (see figure 4 in the supplementary material available at stacks.iop.org/PhysBio/8/026014/mmedia). However, the rate of cell division and apoptosis in the tissue has a more dramatic effect on the diffusion constant. Figure 7 shows that the diffusion constant of cells in a tissue at its homeostatic state is directly proportional to the apoptosis rate k_a. Increasing the noise $k_B T_n$ by two orders of magnitude increases D only by roughly 10%. Hence, the noise intensity appears to only play a marginal role for diffusion. This is an indication that the diffusion of cells arises mainly from a drift in random directions due to cell division and apoptosis. The origin of this effect is discussed in more detail by Ranft *et al* [11].

6. Tissue rheology

We study the rheology of tissues on timescales of the order of the cell cycle time and length scales much larger than single cells. Analytical arguments suggest that tissues behave like fluids on timescales that are long compared to division and apoptosis times. A detailed continuum theory describing this fluidization process is given in [11]. The basic idea in

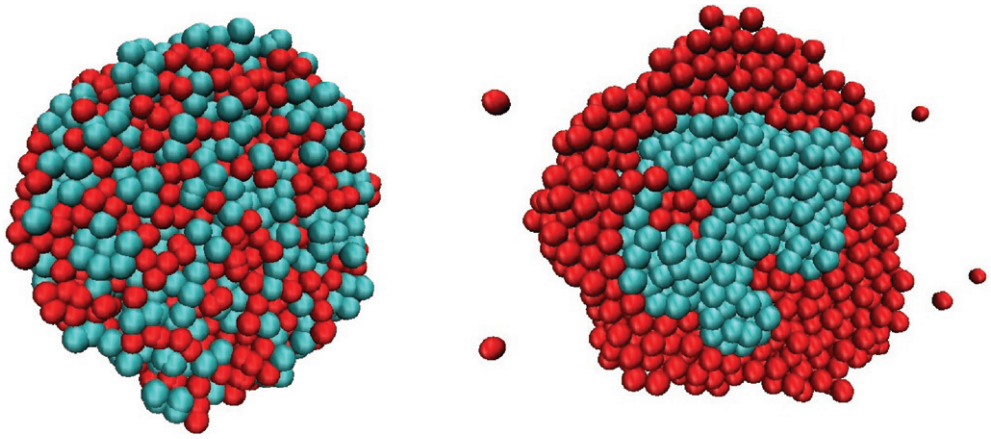

Figure 6. Sorting of two tissues of different adhesive properties with increased noise $k_B T_n^* = 5$. The blue cells adhere to cells of their own species with an adhesion coefficient $f_1^* = 2$; all other adhesions (cross adhesion and self-adhesion for the red tissue) are weaker ($f_1^* = 0.5$). Shown are cuts through the tissue spheroid. (*A*) Initial configuration of the simulation. The two cell types are mixed in a tissue spheroid in free space. (*B*) At the end of the simulation (at $t \approx 39$), the red tissue surrounds the blue tissue. A small number of cells have evaporated off the spheroid.

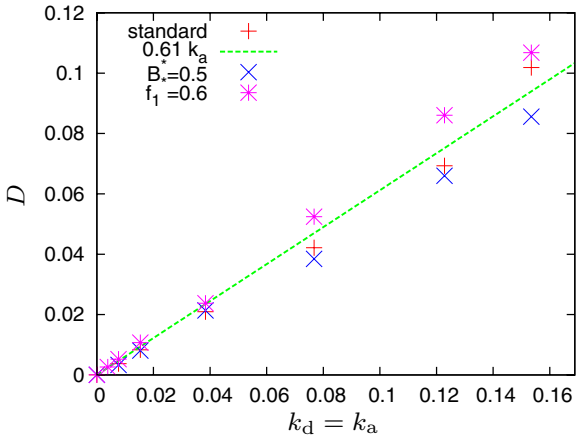

Figure 7. Plot of the diffusion constant of cells in the tissue as a function of the apoptosis rate $k_d = k_a$. The compartment dimensions used are $L_x = L_y = L_z = 4.47$ with periodic boundary conditions. With permission from [11].

this work is that the local homeostatic regulation of a tissue relaxes internal stresses via cell division and apoptosis, which leads to the visco-elastic behavior of otherwise purely elastic tissues. Most importantly, it predicts an inverse proportionality between shear viscosity and cell turnover.

In order to determine the rheological properties of the simulated tissue, we perform a set of simulations closely resembling actual rheological experiments in different ensembles. Our goal is to determine the effective continuum properties of the tissue from given microscopic parameters of our model. We do observe that cell turnover naturally fluidifies tissues on long timescales, and that the general rheological response has a nonlinear dependence on cell turnover, timescales and applied forces.

6.1. Shear plate simulations

As a first type of rheological measurement, we perform *shear plate simulations*. The tissue fills the gap between two infinite parallel plates. The top plate moves at constant velocity relative to the bottom plate, creating a shear profile. The measurement of the stress and velocity profile yields an effective viscosity.

In our simulation, the tissue is confined by two bounce-back walls perpendicular to the z axis, and periodic boundary conditions in the other two directions. The top plate moves at a velocity v_0 in the x-direction. The stress σ_{xz} is measured via the momentum exchange with the walls. The stresses at top and bottom wall are opposite and equal, as expected. The effective viscosity of the tissue is then defined as $\eta = \sigma_{xz}/\dot{\gamma}$, where $\dot{\gamma}$ is the measured velocity gradient in the tissue.

We essentially observe an inverse proportionality between cell turnover and viscosity (see figure 8). At low cell turnover, limitations on simulation time do not allow us to impose shear rates slow enough to be in the 'long time' limit. We observe shear thinning and measure an apparent viscosity independent of the cell turnover rate. This behavior, relevant to the short time behavior of a tissue, is consistent with the observed shear thinning when varying the plate velocity in this regime (see supplementary figures 1–3 available at stacks.iop.org/PhysBio/8/026014/mmedia).

6.2. Bulk-shear simulation

In a second set of simulations, we do not impose a constant shear rate, but a constant shear stress in the bulk of the tissue. For this, the tissue is grown in periodic boundary conditions and a force $\vec{F}$ is exerted directly on each of the two particles constituting a cell. The force density $\vec{f}$ is given by $\vec{f}(\vec{r}) = \rho(\vec{r})\vec{F}(\vec{r})$, where $\rho(\vec{r})$ is the number density of particles at a given point.

We first choose a constant force density, where opposite and equal forces F_0 are exerted in two tissue layers:

$$F_x = \begin{cases} F_0 & \text{if} \quad 0 \leqslant z < d \\ -F_0 & \text{if} \quad L_z/2 \leqslant z < L_z/2 + d \\ 0 & \text{else.} \end{cases} \tag{9}$$

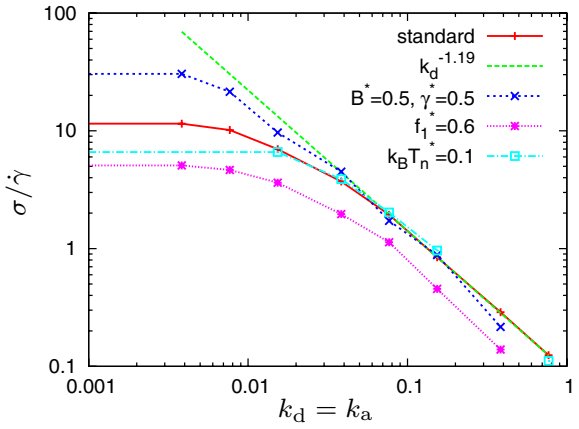

Figure 8. Plots of the ratio of the shear stress σ and the velocity gradient $\dot{\gamma}$ in shear plate simulations for different tissue parameters. The compartment has the dimensions $L_x = L_y = L_z = 5.59$. A top plate velocity $v_0 = 0.17$ was employed. Roughly, the viscosity is inversely proportional to the cell turnover rate. With permission from [11].

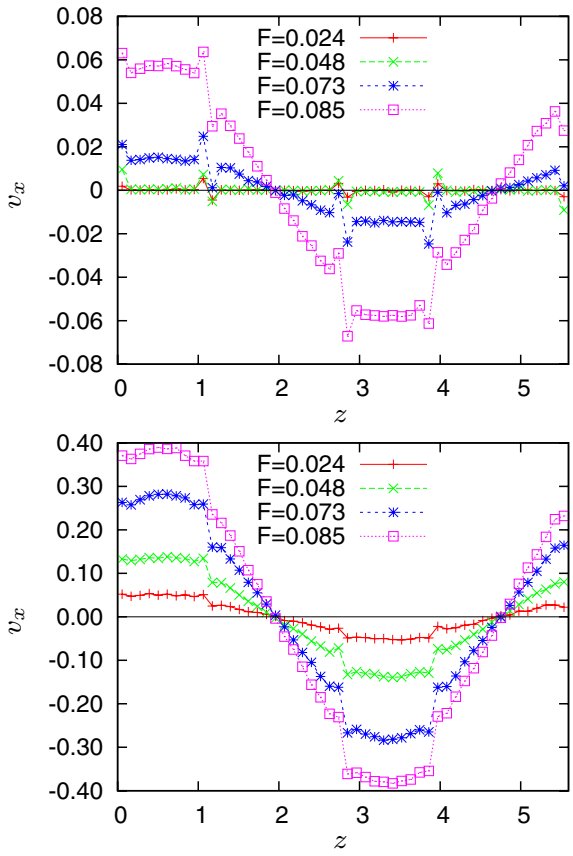

Figure 9. (*A*) Velocity profile of a tissue without apoptosis and cell division in the bulk-shear simulation (achieved by setting $k_a = 0$). The compartment has the dimensions $L_x = L_y = L_z = 5.59$. Over a wide range of forces, the profile vanishes. The force felt by a single cell is given by F. At the force $F = 0.073$, the yield stress threshold is passed and the tissue shows a linear velocity profile in the two regions with no applied force. (*B*) With cell division and apoptosis (standard tissue), any force leads to flow.

In a fluid tissue, a linear profile of the velocity in the x-direction would arise between the two layers in this simulation. We refer to this type of measurement as a *bulk-shear simulation*.

In the absence of cell division and apoptosis ($k_a = 0$), the simulated tissue behaves as a yield-stress fluid. As shown in figure 9, over a wide range of forces, the velocity profile in the tissue vanishes. Only after the yield stress threshold is passed, does the tissue suddenly exhibit a flow. In the presence of apoptosis and cell division, this picture changes dramatically: even for very small shear forces, the tissue shows a linear flow profile; hence, the yield stress vanishes or is very small. As the rate of apoptosis k_a is decreased, the effective viscosity increases and diverges as a power law $k_a^{-\alpha}$. The exponent $1 < \alpha < 1.5$ is close to unity (see figure 12 for a comparison of the different measurement methods).

6.3. Oscillatory shear simulations

To probe the visco-elastic properties of tissues at different timescales, we implement oscillatory shear simulations. We use the same setup as in the bulk shear simulations, but with an oscillating force density given by

$$F_x = F_0 \sin(2\pi z/L_z) \sin(\omega t). \tag{10}$$

The total force exerted on the tissue vanishes, but a shear profile arises at a frequency ω. In the linear regime, the velocity profile is related to the external force by

$$v_x = \mathrm{Re}\left[\frac{\rho F_0 \sin(k_z z)}{\eta_c k_z^2} e^{i\omega t}\right], \tag{11}$$

where Re denotes the real part of a complex number, and η_c is the complex viscosity. We measure η_c in our simulations by fitting equation (11) to the observed velocity profile. In figure 10, the modulus $|\eta_c|$ and the phase δ of the complex viscosity, given by $e^{i\delta} = |\eta_c|/\eta_c$, are plotted as a function of different shear frequencies ω and for different apoptosis rates k_a. Corresponding plots for different noise intensities T_n and adhesion strengths f_1 are given in the supplementary material available at stacks.iop.org/PhysBio/8/026014/mmedia. In all cases, the viscosity decreases with increasing shear frequency as seen in figure 10, whereas the phase angle δ increases toward $\pi/2$. In a Stokes fluid, the *velocity* is proportional to the force ($\delta = 0$), whereas in an elastic material, the *displacement* is proportional to the force ($\delta = \pi/2$). Thus, increasing frequency drives the tissue toward elastic behavior as expected.

6.4. Dynamic tissue compression

While shear simulations can be used to determine the shear viscosities of the tissue, the dynamic bulk modulus must be measured by different means. In addition, the tissue growth rate ($k_d - k_a$) in the vicinity of the homeostatic state as a function of the pressure is essential for mapping our simulations to continuum models introduced in earlier works [9, 11] and must be determined.

To measure these properties, we grow a tissue in a compartment confined by a moving piston, which is used to compress or expand the tissue. A bounce-back wall at $z = 0$ confines the tissue on one side, whereas the piston at $z = z_0(t)$

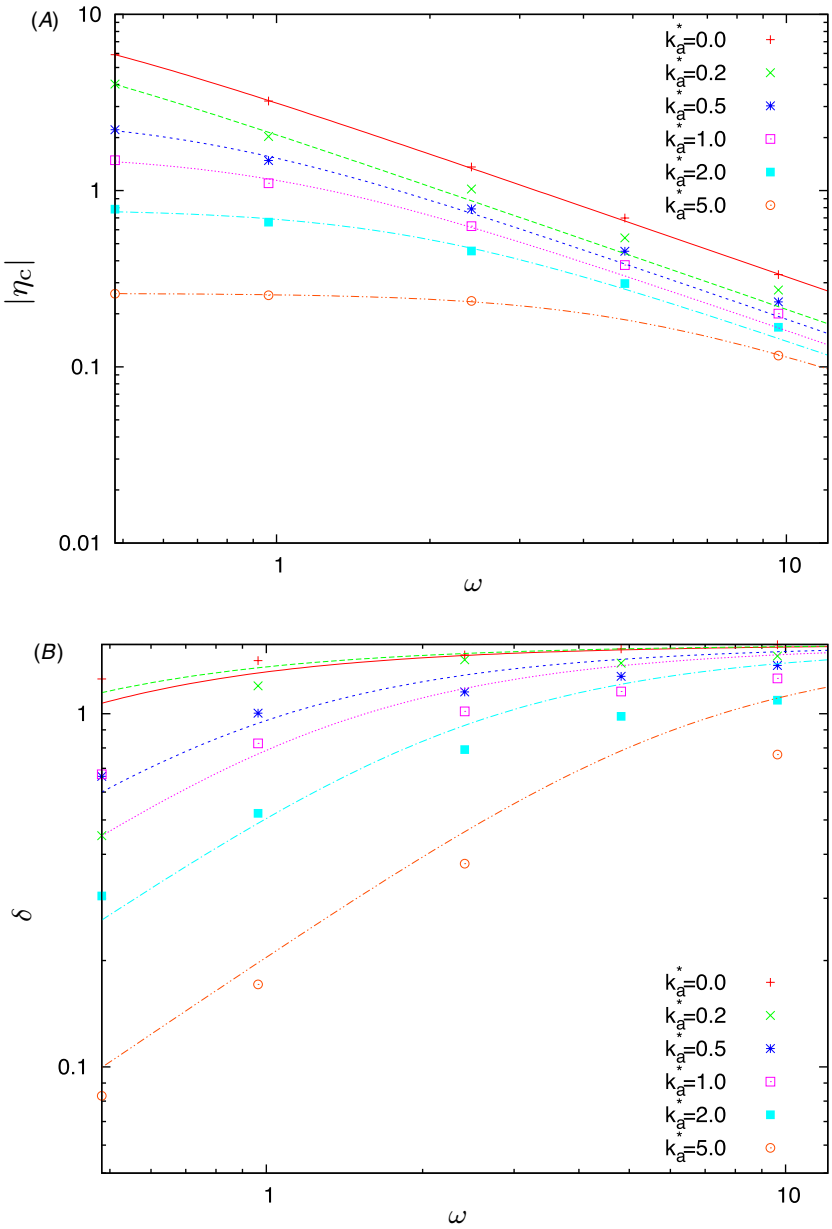

Figure 10. Modulus $|\eta_c|$ (A) and phase δ (B) of the complex viscosity measured in the oscillatory bulk-shear simulation as a function of the shear frequency ω for different apoptosis rates $k_a^* = k_d^*$ in the tissue. Compartment dimensions are $L_x = L_y = L_z = 8.95$. Unless indicated otherwise, the parameters of the standard tissue are used. The amplitude of the force on each particle is set to $F_0 = 0.0076$. A larger viscosity indicates a more solid-like behavior. The value $\pi/2$ is indicated in the plot for the phase (B). A value of $\pi/2$ corresponds to purely elastic behavior, whereas a phase of 0 arises from a purely liquid-like tissue. Increasing cell division and apoptosis clearly leads to a more fluid-like behavior of the tissue. The lines in the plot are fits of the Maxwell model to the data. The complex viscosity is fitted to (A). The fit shown in (B) then directly follows.

is implemented as a force: $F_{z,\text{piston}}(z) = a_{\text{wall}}/(z - z_0)^8$ with $a_{\text{wall}} = 0.093$. Periodic boundary conditions are applied in the two other spatial directions. By changing the compartment volume exponentially via $z_0(t) = z_{\text{init}} \cdot \exp(r\,t)$, a steady-state growth rate r is maintained. The effective growth rate is given by $\partial_t N/N$, and is found to be equal to r for reasonable compression and expansion rates. By running this simulation at different rates r, we probe $(k_d - k_a)$ at different pressures. In cases, where the compression rate $\partial_t z_0/z_{\text{init}}$ exceeds the implemented apoptosis rate k_a, the tissue behaves as an elastic body and the pressure in the tissue diverges as expected.

Otherwise, the pressure and $(k_d - k_a)$ quickly reach a steady state and are combined to give a measurement of the net growth rate $(k_d - k_a)$ as a function of the tissue pressure p (see figure 11(A)). As proposed in [9], $(k_d - k_a)$ is proportional to the difference between the pressure and the homeostatic pressure. These simulations also provide the compressibility of the tissue: since the pressure and the cell density in the tissue do not vary with time, the steady-state density can be expressed as a function of the pressure (see figure 11(B)). Note that this is a dynamic compressibility defined for continuous deformations. Confined to a constant volume, the tissue

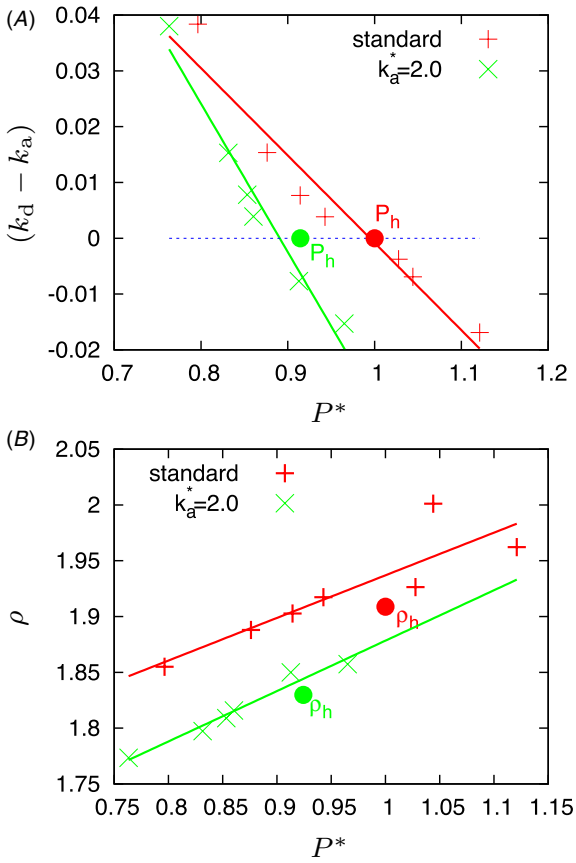

Figure 11. (*A*) Cell division-apoptosis rate as a function of pressure (in the vicinity of the homeostatic state) determined from tissue compression simulations. The curve for the standard tissue is shown together with the curve for the tissue with the twofold apoptosis rate $k_a^* = 2.0$. The growth rate crosses zero at the homeostatic state of the system. (*B*) Steady-state cell density in the tissue plotted as a function of the applied tissue pressure. The curves were determined in the same compression simulations as the data shown in (*A*). A linear fit is also presented. For comparison, pressures obtained from steady-state experiments (see figure 3) representing the homeostatic state are given. Although coming from measurements in different geometries, the homeostatic state variables agree surprisingly well (within less than 10%).

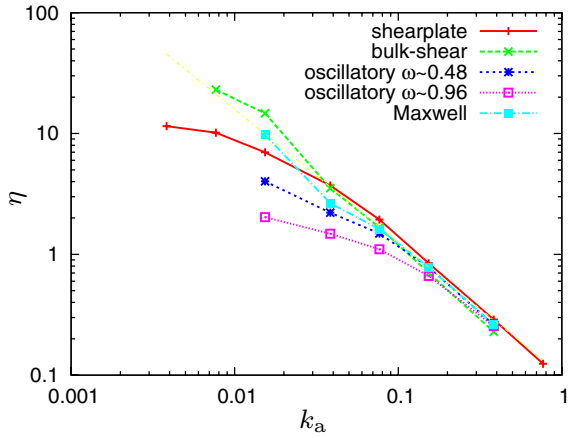

Figure 12. Effective viscosities determined via the shear-plate, the bulk-shear and the oscillatory bulk-shear methods for the standard tissue as a function of k_a. In addition, the viscosities obtained by fitting the Maxwell model in figure 13 are shown. Note how the viscosity obtained by fitting the Maxwell model to the oscillatory shear data nicely agrees with bulk-shear data. For large cell turnover, all methods lead to essentially the same viscosity. At slow cell turnover, shear thinning leads to differences in the measurement techniques.

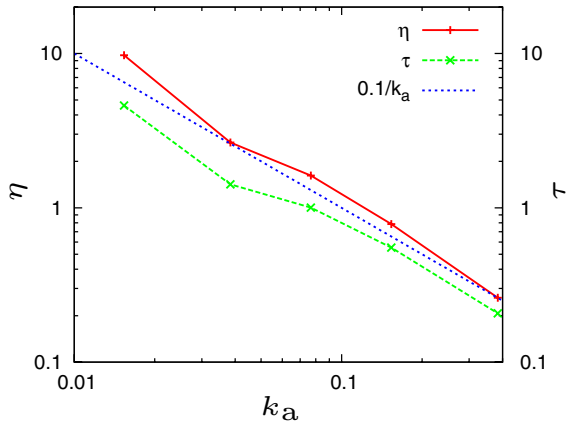

Figure 13. Plot of the parameters of the Maxwell model (fitted to the data presented in figure 10) as a function of k_a. The blue dashed line is proportional to $1/k_a$.

always relaxes to its homeostatic pressure and density. Thus, the long timescale compressibility modulus vanishes.

6.5. *Tissues as Maxwell fluids*

The tissue viscosities obtained in the various simulations are plotted in figure 12 as a function of the apoptosis rate k_a. The various methods give consistent results. At large enough values of k_a, where the tissue behaves as a fluid, the shear viscosity is essentially inversely proportional to the cell turnover (approximately $k_a^{-1.1}$). This is in agreement with the arguments presented by Ranft *et al* [11] which predict $\eta \propto 1/k_a$.

At finite frequency, oscillatory shear simulations show that the tissue is a visco-elastic fluid with a complex viscosity depending on frequency. The simplest model for visco-elastic materials is the Maxwell model, which yields a complex viscosity given by

$$\eta_c = \eta/(1 + i\omega\tau). \tag{12}$$

In this model, the zero-frequency viscosity η and the shear modulus E are related by $\eta = E\tau$, where τ is the visco-elastic relaxation time.

In figure 10, the expressions for the modulus $|\eta_c|$ and the phase δ of the complex viscosity are fitted to the data from oscillatory shear simulations. Although the agreement is not perfect, the main features of the rheological behavior are captured. Both viscosity and viscous relaxation time are inversely proportional to k_a for non-zero k_a (see figure 13) as predicted in [11]. This implies a constant elastic modulus E.

At finite shear stress, shear-thinning effects play a role. In the absence of cell turnover, the tissue behaves as a plastic material with a finite yield stress (see figure 9). Any level of cell turnover fluidizes the tissue on long timescales, and the

yield stress vanishes. The tissue is a non-Newtonian fluid with a viscosity varying with shear rate. Fitting this non-Newtonian behavior with the corotational generalization of the Maxwell model [35, 36], which predicts shear thinning, agreement is only found at low shear rates.

On short timescales, the tissue behaves like a solid, as long as the level of stress in the tissue is below the yield stress threshold. To a first approximation, the timescale, on which the transition between these two regimes takes place, is on the order of the inverse rate of cell division and apoptosis. Note that the rheology at the timescales that we study is a macroscopic property of the tissue. It is dominated by cell turnover, and thus contrary to single-cell experiments where the rheology is dominated by the cytoskeleton [39–41], no power-law dependence of G′ and G″ is found.

7. Concluding remarks

In this work, we introduce a simple particle-based model for simulating tissues. Each cell consists of two particles that repel each other, giving cells the tendency to increase their volume. Cells divide deterministically when reaching a specific size checkpoint. The particles of different cells interact via a pair potential that is repulsive at short distances to model volume exclusion and attractive at intermediate distances to represent cell–cell adhesion. We show that tissues given by this model behave in a realistic manner in many situations and, in particular, possess a well-defined homeostatic state. The homeostatic pressure and density are measured as functions of the model parameters. An important result is that when tissues of different homeostatic pressures undergo a competition in finite volumes, the tissue with the higher homeostatic pressure wins by taking over the compartment. Indeed, we demonstrate that even if the tissue with the lower homeostatic pressure has a much larger unconfined division rate, the tissue with the higher pressure wins the competition. We also show how a higher noise in the tissue—corresponding to a higher cellular mobility for example due to the loss of contact inhibition [37]—leads to an increased homeostatic pressure that could result in neoplastic behavior. Furthermore, adhesive interactions between cells are at the origin of tissue surface tension that cause tissue aggregates to round up. Similarly, interfacial tensions which are responsible for the sorting of mixtures of different cells exist. We measure tissue surface tensions in our simulation as a function of cell–cell adhesion strength.

Using a number of rheological simulations, we measure the visco-elastic properties of the tissue and their dependence on model parameters. The shear viscosity is measured both in a standard shear plate geometry and in a creep configuration in which an external force on the cells is imposed. To further probe the rheology of the tissue, we use an oscillatory shear experiment with a time-dependent external force. Using this technique, we measured the complex viscosity and the loss tangent of the tissue. All three techniques lead to compatible results. In particular, we investigate the dependence of the rheological properties on the strength of cell–cell adhesion f_1, the level of noise T_η and the rate of apoptosis k_a in the tissue. Both the lower levels of cell–cell adhesion and the higher levels of noise lead to more fluid-like behavior of the tissue; the shear viscosity η, the modulus of the complex viscosities $|\eta_c|$, as well as the phase shift δ decreases. The apoptosis rate in the tissue has an even more dramatic effect on tissue rheology: for a vanishing apoptosis rate, the tissue has a finite yield stress and exhibits typical plastic behavior, while for a non-zero rate of apoptosis, the yield stress vanishes. Hence, cell division and apoptosis lead to fluidization of the tissue. We find that the shear viscosity decreases with the apoptosis rate with a power law close to $1/k_a$.

We also study the diffusion of cells within the tissue: in parameter regimes where the fluidization of the tissue is caused by cell division and apoptosis, the diffusion constant in the tissue is directly proportional to the rate of cell division and apoptosis, while most other tissue parameters do not seem to affect it significantly. Finally, we present a number of simulations, in which we compress the tissue dynamically in a controlled manner. Using these simulations, we determine both its dynamical compressibility and its response to imposed pressure via cell division and apoptosis. In our simulations, we therefore measure all the continuum properties of the tissue required for applying the coarse-grained models introduced in earlier works [9].

In further research, we would like to use these simulations to study more complex tissue architectures such as multi-layered epithelia. In particular, the internal organization of these tissues with respect to populations of stem cells and differentiation should be investigated. The development of spatial organization within tissues such as the finger-like protrusions occurring in the epidermis could also be studied. The stability of these structures under perturbations is an important question, for example, how do different subpopulations of cells coexist in these tissues and what is the origin of fingering instabilities, which are observed at many tissue interfaces in malignant and premalignant epithelia. Finally, the survival of mutated cells and the dynamics of tissue competition should be studied in tissues with a more complex structure like epithelia and nutrient-limited tumors.

References

[1] Théry M, Jiménez-Dalmaroni A, Racine V, Bornens M and Jülicher F 2007 Experimental and theoretical study of mitotic spindle orientation *Nature* **447** 493–6

[2] Whitehead J, Vignjevic D, Fütterer C, Beaurepaire E, Robine S and Farge E 2008 Mechanical factors activate β-catenin-dependent oncogene expression in APC1638N/+ mouse colon *HFSP J.* **2** 286

[3] Engler A J, Sen S, Sweeney H L and Discher D E 2006 Matrix elasticity directs stem cell lineage specification *Cell* **126** 677–89

[4] Foty R A, Forgacs G, Pfleger C M and Steinberg M S 1994 Liquid properties of embryonic tissues: measurement of interfacial tensions *Phys. Rev. Lett.* **72** 2298–301

[5] Foty R A, Pfleger C M, Forgacs G and Steinberg M S 1996 Surface tensions of embryonic tissues predict their mutual envelopment behavior *Development* **122** 1611–20

[6] Duguay D, Foty R A and Steinberg M S 2003 Cadherin-mediated cell adhesion and tissue segregation: qualitative and quantitative determinants *Dev. Biol.* **253** 309–23

[7] Fung Y C 1993 *Biomechanics: Mechanical Properties of Living Tissues* (Berlin: Springer)

[8] Guevorkian K, Colbert M J, Durth M, Dufour S and Brochard-Wyart F 2010 Aspiration of biological viscoelastic drops *Phys. Rev. Lett.* **104** 218101

[9] Basan M, Risler T, Joanny J F, Sastre-Garau X and Prost J 2009 Homeostatic competition drives tumor growth and metastasis nucleation *HFSP J.* **3** 265–72

[10] Basan M, Joanny J F, Prost J and Risler T 2011 Undulation instability of epithelial tissues *Phys. Rev. Lett.* accepted

[11] Ranft J, Elgeti J, Basan M, Joanny J F, Prost J and Jülicher F 2010 Fluidization of tissues by cell division and apoptosis *Proc. Natl Acad. Sci.* **107** 20863–8

[12] Drasdo D, Kree R and McCaskill J S 1995 Monte Carlo approach to tissue-cell populations *Phys. Rev.* E **52** 6635–57

[13] Drasdo D 2000 Buckling instabilities of one-layered growing tissues *Phys. Rev. Lett.* **84** 4244–7

[14] Drasdo D and Loeffler M 2001 Individual-based models to growth and folding in one-layered tissues: intestinal crypts and early development *Nonlinear Anal., Theory Methods Appl.* **47** 245–56

[15] Drasdo D and Hohme S 2003 Individual-based approaches to birth and death in avascu1ar tumors *Math. Comput. Model.* **37** 1163–76

[16] Drasdo D and Höhme S 2005 A single-cell-based model of tumor growth *in vitro*: monolayers and spheroids *Phys. Biol.* **2** 133–47

[17] Galle J, Loeffler M and Drasdo D 2005 Modeling the effect of deregulated proliferation and apoptosis on the growth dynamics of epithelial cell populations *in vitro* *Biophys. J.* **88** 62–75

[18] Galle J, Aust G, Schaller G, Beyer T and Drasdo D 2006 Individual cell-based models of the spatio-temporal organisation of multicellular systems-achievements and limitations *Cytometry* **69** 704–10

[19] Drasdo D, Hoehme S and Block M 2007 On the role of physics in the growth and pattern formation of multi-cellular systems: What can we learn from individual-cell based models? *J. Stat. Phys.* **128** 287–345

[20] Hengstler J G, Drasdo D and Gebhardt R 2007 Liver regeneration after intoxication with CCl4: spatial-temporal mathematical modelling in triple transgenic mice *Toxicol. Lett.* **172** 46

[21] Höhme S, Hengstler J G, Brulport M, Schäfer M, Bauer A, Gebhardt R and Drasdo D 2007 Mathematical modelling of liver regeneration after intoxication with CCl4 *Chem. Biol. Interact.* **168** 74–93

[22] Brú A, Pastor J M, Fernaud I, Brú I, Melle S and Berenguer C 1998 Super-rough dynamics on tumor growth *Phys. Rev. Lett.* **81** 4008–11

[23] Brú A, Albertos S, Subiza J Luis, García-Asenjo J L and Brú I 2003 The universal dynamics of tumor growth *Biophys. J.* **85** 2948–61

[24] Schaller G and Meyer-Hermann M 2005 Multicellular tumor spheroid in an off-lattice Voronoi–Delaunay cell model *Phys. Rev.* E **71** 51910

[25] Freyer J P and Sutherland R M 1985 A reduction in the *in situ* rates of oxygen and glucose consumption of cells in EMT 6/Ro spheroids during growth *J. Cell. Physiol.* **124** 516–24

[26] Freyer J P and Sutherland R M 1986 Regulation of growth saturation and development of necrosis in EMT6/Ro multicellular spheroids by the glucose and oxygen supply *Cancer Res.* **46** 3504

[27] Sandersius S A and Newman T J 2008 Modeling cell rheology with the Subcellular Element Model *Phys. Biol.* **5** 015002

[28] Pathmanathan P, Cooper J, Fletcher A, Mirams G, Murray P, Osborne J, Pitt-Francis J, Walter A and Chapman SJ 2009 A computational study of discrete mechanical tissue models *Phys. Biol.* **6** 036001

[29] Wells W A 2002 Does size matter? *J. Cell Biol.* **158** 1156

[30] Nikunen P, Karttunen M and Vattulainen I 2003 How would you integrate the equations of motion in dissipative particle dynamics simulations? *Comput. Phys. Commun.* **153** 407–23

[31] Foty R A and Steinberg M S 2005 The differential adhesion hypothesis: a direct evaluation *Dev. Biol.* **278** 255–63

[32] Rieu J P, Kataoka N and Sawada Y 1998 Quantitative analysis of cell motion during sorting in two-dimensional aggregates of dissociated hydra cells *Phys. Rev.* E **57** 924–31

[33] Rieu J P, Upadhyaya A, Glazier J A, Ouchi N B and Sawada Y 2000 Diffusion and deformations of single hydra cells in cellular aggregates *Biophys. J.* **79** 1903–14

[34] Upadhyaya A, Rieu J P, Glazier J A and Sawada Y 2001 Anomalous diffusion and non-Gaussian velocity distribution of Hydra cells in cellular aggregates *Physica A* **293** 549–58

[35] Larson R G 1988 *Constitutive Equations for Polymer Melts and Solutions* (Boston, MA: Butterworths)

[36] Kruse K, Joanny J F, Jülicher F, Prost J and Sekimoto K 2005 Generic theory of active polar gels: a paradigm for cytoskeletal dynamics *Eur. Phys. J.* E **16** 5–16

[37] Basan M, Idema T, Lenz M, Joanny J F and Risler T 2010 A reaction-diffusion model of the cadherin–catenin system: a possible mechanism for contact inhibition and implications for tumorigenesis *Biophys. J.* **98** 2770–9

[38] Humphrey William, Dalke Andrew and Schulten Klaus 1996 VMD—visual molecular dynamics *J. Mol. Graph.* **14** 33–8

[39] Hoffman B, Massiera G, Citters K Van and Crocker J C 2006 The consensus mechanics of cultured mammalian cells *Proc. Natl Acad. Sci.* **103** 10259–64

[40] Fabry B, Maksym G N, Butler J P, Glogauer M, Navajas D and Fredberg J J 2001 Scaling the microrheology of living cells *Phys. Rev. Lett.* **87** 148102

[41] Stamenovic D, Suki B, Fabry B, Wang N and Fredberg J J 2004 Rheology of airway smooth muscle cells is associated with cytoskeletal contractile stress *J. Appl. Physiol.* **96** 1600–5